Conformational Dynamics of DnaB Helicase upon DNA and Nucleotide Binding: Analysis by Intrinsic Tryptophan Fluorescence Quenching[†,‡]

Stephen Flowers,[§,||] Esther E. Biswas,[§,||] and Subhasis B. Biswas*[,§]

Department of Molecular Biology, School of Osteopathic Medicine & Graduate School of Biomedical Sciences, University of Medicine & Dentistry of New Jersey, Stratford, New Jersey 08084, and Program in Biotechnology, Department of Laboratory Sciences, Thomas Jefferson University, Philadelphia, Pennsylvania 19107

Received April 22, 2002; Revised Manuscript Received December 20, 2002

ABSTRACT: DnaB helicase of *E. coli* unwinds duplex DNA in the replication fork using the energy of ATP hydrolysis. We have analyzed structural and conformational changes in the DnaB protein in various nucleotides and DNA bound intermediate states by fluorescence quenching analysis of intrinsic fluorescence of native tryptophan (Trp) residues in DnaB. Fluorescence quenching analysis indicated that Trp48 in domain α is in a hydrophobic environment and resistant to fluorescence quenchers such as potassium iodide (KI). In domain *β*, Trp294 was found to be in a partially hydrophobic environment, whereas Trp456 in domain *γ* appeared to be in the least hydrophobic environment. Binding of oligonucleotides to DnaB helicase resulted in a significant attenuation of the fluorescence quenching profile, indicating a change in conformation. ATP*γ*S or ATP binding appeared to lead to a conformation in which Trp residues had a higher degree of solvent exposure and fluorescence quenching. However, the most dramatic increase of Trp fluorescence quenching was observed with ADP binding with a possible conformational relaxation. Site-specific Trp → Cys mutants of DnaB helicase demonstrated that conformational change upon ADP binding could be attributed exclusively to a conformational transition in the α domain leading to an increase in the solvent exposure of Trp48. However, formation of DnaB·ATP*γ*S·DNA ternary complex led to a conformation with a fluorescence quenching profile similar to that observed with DnaB alone. The DnaB·ADP·DNA ternary complex produced a quenching curve similar to that of DnaB·ADP complex pointing to a change in conformation due to ATP hydrolysis. There are at least four identifiable structural/conformational states of DnaB helicase that are likely important in the helicase activity. The noncatalytic α domain in the N-terminus appeared to undergo the most significant conformational changes during nucleotide binding and hydrolysis. This is the first reported elucidation of the putative role of domain α, which is essential for DNA helicase action. We have correlated these results with partial structural models of α, *β*, and *γ* domains

DnaB helicase is the primary replicative DNA helicase in *E. coli* and is known to play a pivotal role in chromosomal DNA replication (*1*−*10*). The helicase activity of DnaB was first elucidated in studies carried out by LeBowitz and McMacken (*5*). DnaB helicase is a 5′ → 3′ helicase that appears to migrate along the lagging strand. It is a DNA dependent ATPase and a DNA helicase; consequently, it interacts with nucleotides and ssDNA. It is also involved in assembling the replisome in *Escherichia coli* and *λ* bacteriophage DNA replication. DnaB helicase appears to interact physically and functionally with DNA template and various *E. coli* replication proteins such as DnaA, DnaC, DnaG primase, and the *τ* subunit of polymerase III holoenzyme forming the replisome (*11*−*22*). In repair mechanisms, DnaB helicase interacts with the proteins of the replisome, including PriA, PriB, and DnaT. DnaB has also been shown to interact physically with *λ*P, *λ*O proteins in the initiation of *λ* DNA replication (*5*, *6*, *17*). It has a strong DNA-dependent ATPase activity that provides energy for DNA unwinding (*23*). We have shown earlier that DnaC and *λ*P proteins attenuate DNA dependent ATPase activity of DnaB protein by physically interacting with the helicase (*7*). Furthermore, DnaB helicase modulates enzymatic activities of a number of DNA replication proteins including DNA primase and pol III holoenzyme (*17*−*22*).

DnaB helicase is a hexamer composed of six identical monomers. The hexamer appears to bind three nucleotides per hexamer with high affinity and possibly three more with low affinity (*23*). It also binds a maximum of three oligonucleotides per hexamer (*24*, *25*). The primary structure of DnaB helicase consists of 471 amino acids with three tryptophan residues; W-48, W-294, and W-456 (*1*, *4*). Previously, we have shown that DnaB helicase is composed of three functional domains: α, *β*, and *γ* (*24*−*25*). Domain α includes amino acid residues 1−156 and has no known enzymatic activity or structural motif. It is also the least conserved of the three domains of DnaB. Domain *β* is comprised of residues 157−300 and harbors the ATPase active site. Domain *γ* is the most highly conserved among the three domains and consists of residues 301−471. Domain

[†] This work was supported by a grant from the National Institute of General Medical Sciences/National Institutes of Health (GM 36002-13) and funds from the Dean of the School of Medicine.

[‡] Submitted in partial fullfilment of the Masters of Science degree in Biotechnology, Thomas Jefferson University.

* Corresponding author. Phone: (856) 566-6270. Fax 781-207-8476. E-mail: subhasis.biswas@umdnj.edu.

[§] University of Medicine & Dentistry of New Jersey.

[||] Thomas Jefferson University.

10.1021/bi025992v CCC: $25.00
Published on Web 01/28/2003

γ is the DNA binding domain that positively regulates the ATPase activity of the β domain (*24*, *25*). Our previous studies demonstrated that there is a leucine zipper at the C-terminus of the γ domain (*24*−*25*) that is likely involved in dimerization and DNA binding. Further upstream of the leucine zipper, a basic RxRxRR motif is present that is involved in DNA binding, as demonstrated by in vitro site-specific mutagenesis (*25*).

Tryptophan is the least abundant amino acid in proteins and is the most widely used in intrinsic fluorescence analysis as reporter groups for protein conformational change (*27*−*29*). Steady-state fluorescence quenching of intrinsic Trp fluorescence has been used to study dynamic conformational changes in proteins and to assess the environments of Trp residues in a variety of proteins (*27*−*29*). Chemical agents such as iodide or acrylamide can quench the intrinsic Trp fluorescence, the extent of which depends on the exposure of the indole moiety of Trp residue to the solvent. By analyzing the efficiency of quenching, alterations in the molecular environment of each Trp residue due to protein conformational changes can be determined even when the conformational changes are small and local (*28*). Iodide is a very ionic species that will only quench the fluorescence of Trp residues that are located in more hydrophilic environments of proteins particularly on the surface, while acrylamide readily penetrate in the hydrophobic interior and quenches fluorescence emission of Trp residues less discriminately (*28*).

We have analyzed structural and conformational changes in the DnaB protein that occur upon nucleotide and DNA binding by fluorescence emission quenching studies involving its three tryptophan (Trp) residues. The three native Trp residues in DnaB are uniquely located, one each in the α (Trp48), β (Trp294), and γ (Trp456) domains of DnaB. The unique locations of the three Trp residues on each of α, β, and γ domains of the DnaB protein made these residues highly suitable for use as fluorescent reporter groups to probe conformational changes associated with nucleotide and DNA binding and correlated with possible conformational changes that may occur during enzymatic DNA unwinding.

MATERIALS AND METHODS

Nucleic Acids, Enzymes, and Other Reagents. Oligonucleotides were synthesized by Integrated DNA Technologies (Coralville, IO). Potassium iodide was obtained from Aldrich Chemicals. Low fluorescence 1M stock solutions of potassium phosphate were obtained from PanVera Corporation (Madison, WI). HPLC-grade water was obtained from Fisher Chemicals.

Construction, Expression, and Purification of Wild Type and Deletion Mutants of DnaB. The plasmids pDnaB1 (pET29bDnaB expressing wild-type DnaB) and pDnaBΔ1 (C-terminal deletion mutant) were constructed as described previously (*24*, *25*). The C-terminal deletion mutant DnaBΔ1 lacked 55 amino acid residues in the C-terminal and the polypeptide ended with Ile416. The PCR amplification and construction of pDnaBΔ1plasmid has been described in a previous publication (*25*). We have demonstrated earlier that despite the lack of 55 amino acid C-terminus, it retained DNA-stimulated ATPase activity, and somewhat attenuated DNA binding and DNA helicase activities (*25*).

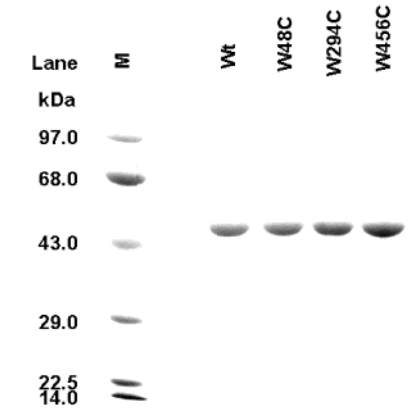

FIGURE 1: SDS−polyacrylamide gel of wild type and mutant DnaB proteins. Approximately 5 μg of highly purified DnaB helicase and mutant proteins were loaded on the gel. The gel was electrophoresed and was stained with Coomassie brilliant blue R-250.

Buffers. Buffer A contained 25 mM Tris-HCl (pH 7.9), 10% sucrose and 250 mM NaCl. Buffer B contained 25 mM Tris-HCl (pH 7.5), 10% (v/v) glycerol, 1 mM DTT, 5 mM $MgCl_2$, and 100 mM KCl as indicated. Buffer C contained 25 mM KH_2PO_4, 120 mM NaCl, and 5 mM $MgCl_2$. All buffers were prepared for fluorescence studies with HPLC-grade water with low background fluorescence.

Construction of DnaB W → C Mutants, Protein Expression, and Purification. The DnaB helicase was expressed using a T7 expression system, pDnaB1 (pET29b-DnaB), that has been described earlier (*24*). The pDnaB1 plasmid was mutagenized using the indicated oligonucleotides following the Quick Change XL mutagenesis protocol (*25*). Mutants were verified by DNA sequencing. We have constructed three W → C mutants: pDnaB1W48C, pDnaB1W294C, and pDnaB1W456C. Each of these mutants was introduced in *E. coli*, BL21[DE3] cells and expressed using 0.1 mM IPTG induction. All three mutants produced soluble protein (Figure 1). The wild type and mutant proteins were expressed and purified similarly to homogeneity. The SDS−PAGE analysis of the purified proteins is presented in Figure 1.

Site-Directed Mutagenesis of the DnaB Helicase. Site-directed mutagenesis was carried out using Quick Change XL kit (Stratagene Inc., La Jolla, CA). The DnaB expression plasmid pDnaB1 was used as a template to produce the following mutants, pDnaBW48C, pDnaBW294C, and pDnaBW456C. PCR was carried out for 18 cycles, and each cycle was 50 s at 95 °C, 50 s at 60 °C, and 2 min at 68 °C using the oligonucleotide pairs 5′-CTA GAT AAC GAA CGC TGC GAT GAT GTA GCC GAG CG-3′ and 5′ CGC TCG GCT ACA TCA TCG CAG CGT TCG TTA TCT AG-3′ for DnaBW48C, 5′ CTC GAT GAC GAA GAC TGC GCG CGC ATT TCC GGC AC-3′ and 5′ GTG CCG GAA ATG CGC GCG CAG TCT TCG TCA TCG AG-3′ for DnaBW294C, and 5′-CTT TAA CGG TCA ATG CTC GCG CTT CGA CAA CTA-3′ and 5′-CAT AGT TGT CGA AGC GCG AGC ATT GAC CGT TAA AG-3′ for DnaBW456C.

Protein Expression and Purification. Expression of proteins was accomplished through the use of a T7 expression system. The genes encoding these proteins were cloned into the inducible expression vector pET29b, (Novagen Corp., Milwaukee, WI). Constructs, pDnaB1 and pDnaBΔ1, and the mutant plasmids were then transformed in the inducible *E. coli* stain BL21 (DE3). The *E. coli* cells harboring

expression plasmids were grown to OD 0.4, induced with 0.1 mM IPTG for 3 h, and harvested.

Purification of the proteins was carried out according to our standard protocol (*30*). *E. coli* pellets were suspended in 0.2 mg/mL lysozyme, 0.25 M NaCl, 2 mM spermidine, and 5 mM $MgCl_2$ and then incubated on ice for 30 min. This was followed by 5 min incubation at 37 °C. Further disruption of the cell membrane was achieved using sonication. An additional 0.5 M NaCl was added to the homogenate, and after 1 h of incubation at 4 °C, it was centrifuged at 18 500 rpm for 30 min. The supernatant was then precipitated with 0.18 g/mL ammonium sulfate for 1 h at 4 °C. The supernatant was centrifuged at 18 500 rpm for 30 min, and the resulting protein pellet was resuspended in buffer A and dialyzed. The protein was loaded onto a POROS-Q column (10 mg protein/mL of resin) equilibrated with buffer A containing 100 mM NaCl (buffer A100). The column was washed with buffer A200. A gradient from A200 to A500 was used to elute the column, and peak fractions were collected. Protein concentrations were measured spectrophotometrically by absorption at 280 nm UV. Purity was monitored by SDS−PAGE electrophoresis.

DNA Helicasce Assays. The DNA helicase assays were carried out as described earlier (*24*) and briefly described below. The substrate was prepared by hybridizing a synthetic 60-mer oligonucleotide to M13mpl9 ssDNA. The oligonucleotide is complementary to a 50 bp sequence between nucleotides 6268 and 6317 of M13mp19 ssDNA and contained 5 nucleotide tails (nonhomologous regions) on both 5′ and 3′ termini and described in detail earlier (*34*). The purified substrate was diluted to a final concentration of 17-fmol/μL (10 000−20 000 cpm/μL) with 10 mM Tris·HCl (pH 7.5), 1 mM EDTA.

Reaction mixtures were set up on ice as follows. A standard 20 μL reaction volume contained buffer A, 10 mM $MgCl_2$, 3.4 mM ATP, 100 μg/mL each BSA and *E. coli* SSB, 17 fmol (10 000−20 000 cpm/μL) of substrate and the indicated amount of DnaB protein or mutant proteins. The mixtures were incubated at 37 °C for the times indicated, and the reactions were terminated by the addition of 4 μL of 2.5% SDS, 60 mM EDTA, and 1% bromophenol blue. A fraction (25%) of each reaction mixture was analyzed on 8% polyacrylamide gels in 1X TBE and 0.1% SDS. The electrophoresis was carried out in 1X TBE, 0.1% SDS for 1 h at 160 V. Following electrophoresis the gels were dried and exposed to Fuji RX film at −80 °C for 12 h. The intact hybridized oligonucleotide with the M13mp19 DNA migrated as a high molecular weight species, whereas the unhybridized oligonucleotide that resulted due to the action of DNA helicase migrated as a low molecular weight species. The results of these assays are shown in Figure 2.

Steady-State Fluorescence Measurements. Steady-state fluorescence was performed with either a LS50B (Perkin-Elmer Inc., Shelton, CT) or a custom-made photon-counting spectrofluorometer at ambient temperature. Excitation wavelength was set to 295 nm to avoid excitation of either tyrosine or phenylalanine residues. Emission was scanned from 320 to 400 nm. Excitation and emission slits were set at 8 nm and 4 nm respectively. All spectroscopic measurements were carried out in buffer C. Stock solutions of 7 M urea, 5 M KI, and 5 M acrylamide were prepared in buffer C. Sodium thiosulfate (200 μM) was added to solutions of KI to avoid

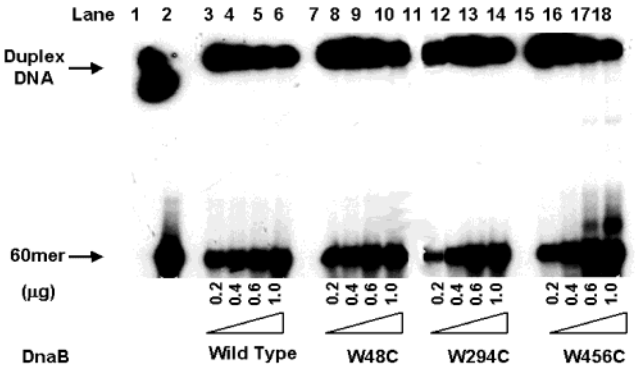

FIGURE 2: Analysis of the DNA helicase activities of the DnaB protein and W → C mutants. Standard DNA helicase assays were carried out as described in Materials and Methods. Titrations for each mutant were carried in the range of 0.2−1 μg protein per assay (0.4−2 μM final concentration as monomer). The substrate is a 60-mer oligonucleotide labeled with ^{32}P at the 5′ end and hybridized to M13mp19 ssDNA with a five nucleotide nonhomologous regions at each end. The 60-mer oligonucleotide produced by DnaB helicase unwinding is shown in the bottom of the autoradiogram. In lanes 17 and 18, a second band was observed, which is occasionally observed due to incomplete denaturation of SSB·oligonucleotide complex, generated during DNA helicase action, by sodium dodecyl sulfate in the helicase stop buffer.

the formation of I_3^-, which absorbs at the same wavelength of tryptophan fluorescence. The spectra presented were the average of three to four scans and were also corrected for background.

Quenching Studies Using Potassium Iodide and Acrylamide. To determine the hydrophobicity of environment solvent exposure of each tryptophan residue, fluorescence quenching analysis was performed using wild-type DnaB and mutated DnaB proteins. Titrations for wild type and mutant DnaB proteins (100μg/mL) were carried out in 25 mM Tris·HCl (pH 7.5), 10% glycerol, 5 mM $MgCl_2$, 150 mM KCl. Reactions were carried out, at 20 °C, in separate culture tubes. In experiments involving nucleotide or oligonucleotides cofactors, the reaction was incubated at room temperature for 20 min to allow for binding to reach equilibrium. Then increasing concentrations of quencher (KI or acrylamide) ranging from 0 to 0.5 M were added. KCl was added so that total salt (KI + KCl) concentration remained constant and equal to the highest concentration of KI used in the experiment.

From the recorded titration spectra, the rate of quenching and the accessibility of tryptophan were calculated using Stern−Volmer and Lehrer equations, respectively (eqs 1 and 2). To determine the Stern−Volmer plot with total tryptophan accessibility, fluorescence quenching analysis was carried out using potassium iodide as a quencher as described above with 100 μg/mL DnaB protein in buffer B containing 7 M urea and titrated with 5 M KI to a final concentration of 0.5 M.

Fluorescence quenching data were analyzed by the Stern−Volmer equation as described by Lakowicz (*28*):

$$(F_0/F) - 1 = K_a \cdot [Q] \quad (1)$$

where F_0 and F are the fluorescence intensities in the presence and absence of the quencher, respectively. [Q] is the concentration of the quencher. K_a is the Stern−Volmer constant, which is a direct measure of the quenching efficiency. If a plot of (F_0/F) versus [Q] yields a linear plot,

the K_a can be obtained from the slope. A nonlinear plot is indicative of the presence of multiple components with multiple values of K_a.

In proteins that contain multiple tryptophan residues, there are often significant differences in the accessibility of different Trp residues to the solvent reflecting local protein conformation that lead to deviations from linearity in the Stern−Volmer plot. The fraction of tryptophan accessible to the quencher can be calculated by using the Lehrer eq 2, a modification of the Stern−Volmer equation:

$$\frac{F_0}{\Delta F} = \frac{1}{f_a K_a} \cdot \frac{1}{[Q]} + \frac{1}{f_a} \qquad (2)$$

where ΔF is $F_0 - F$ and f_a represents the fraction of tryptophan residues that are accessible to solvent and fluorescence quenching and can be calculated from the *y*-intercept of the Lehrer plot $\{F_0/\Delta F$ vs $1/[Q]\}$.

It is important to note that complexes of DnaB with nucleotides and/or oligonucleotides need to be formed at a salt concentration of ≤0.1 M KCl or KI. Once the complex was formed, it remained stable at higher salt concentration up to 0.5 M.

Fluorescence Measurements of DnaB Helicase and Substrate Interactions. All fluorescence measurements were made at ambient temperature (~20 °C). We analyzed the effects of DNA and ATP binding on the conformation of DnaB helicase by measuring changes in the tryptophan environment by fluorescence quenching analysis. Iodide quenching of tryptophan fluorescence of DnaB protein (100 μg/mL) was performed by titration with 5 M KI up to a final concentration of 0.5 M in the presence of either 130 nM oligo$(dT)_{25}$, 1 mM ATPγS, or 1 mM ADP as indicated. Iodide quenching of tryptophan fluorescence was then performed using a combination of 130 nM oligo$(dT)_{25}$ with either 1 mM ATPγS or 1 mM ADP. ATPγS was chosen for these studies as a nonhydrolyzable form of ATP, making it possible to attribute changes in iodide quenching to the binding of ATP without interference from ATP hydrolysis. We have also measured DNA binding kinetics under the experimental conditions by gel retardation analysis (*11*, *12*) and determined the binding to be complete in less than 5 min (data not shown).

To study the effects of DNA binding by means of tryptophan quenching, titrations were carried out by maintaining the concentration of iodide at 100 mM and varying the concentration of the respective ligand (oligonucleotides or nucleotide triphosphates). DnaB concentrations were maintained at 100 μg/mL and the iodide concentration was maintained at 100 mM. Oligo(dT) of various lengths 25, 15, 10, or 6 residues were used to examine both binding and the minimum size needed to cause changes in the tryptophan fluorescence. Nucleotide binding studies with ATPγS and ADP were carried out similarly.

Complexes of DnaB helicase with various substrates were prepared in the absence of added KI. Once the complex is formed, the titration was carried with KI. DnaB does not bind DNA at high salts (>200 mM KCl), but once the complex is formed it does not dissociate from the substrate with salt concentration below 500 mM. All of these experiments were carried out by first forming the complex in the absence of KI.

Homology-Based Modeling. Homology-based modeling of DnaBβγ polypeptide was carried out in several discreet steps. First, we aligned the polypeptide sequence with the X-ray structure of T7 gene 4 helicase domain and available crystallographic coordinates. Preliminary structure was generated using Swiss-PDB program. This structure was further refined by using SYBYL6.7 software (Tripos Inc., St. Louis, MO).

Other Methods. Protein concentrations were determined by two methods. The Bradford assay using bovine serum albumin as a standard and the extinction coefficient method, where $\epsilon_m^{280} = 1.85 \times 10^5\ M^{-1}$ in 50 mM Tris-HCl (pH 7.5) for wild-type DnaB protein.

RESULTS

DNA Helicase Activity of DnaB Proteins and Its Mutants. We have constructed, expressed, and purified a number of tryptophan W → C mutants of DnaB helicase (Figure 1). It was not clear whether the W → C mutations would affect the enzymatic activities of DnaB. Consequently, we have analyzed the DNA helicase activities of the mutants and the wild type using a standard DNA helicase assay. The results of the DNA helicase assay, presented in Figure 2, demonstrated that all of three W → C mutants were fully active as DNA helicase and were comparable to the wild-type DnaB. Therefore, none of these mutations appeared to cause drastic structural or conformational perturbation in DnaB mutants.

The Molecular Environments of Tryptophan Residues in DnaB Helicase Are Uniquely Different. Tryptophan residues (Trp) in proteins are normally of infrequent occurrence and have diverse local molecular environments that can range from hydrophilic to hydrophobic. In addition, the indole group in Trp is a fluorescent group that can be specifically excited by 295 nm wavelengths, and the emission spectrum is normally observed between 320 and 400 nm without interference from more commonly occurring tyrosine and phenylalanine groups. These properties enable Trp to be used as a probe for detecting and determining the nature of internal conformational transitions in proteins during binding of various ligands and enzymatic catalysis (*28*). Detailed analysis of the patterns of quenching of Trp fluorescence using collisional quenchers, particularly iodide, allows evaluation of changes in the hydrophobicity of the local environment of the indole moiety within a protein as well as changes due to induced alterations in protein conformation. Our approach here has been to first define the environments of each of the Trp residues by fluorescence quenching using iodide and then to determine the effects of site-directed mutagenesis or deletion of protein segments on the Trp environment.

We have examined iodide quenching of Trp residues in both native and denatured DnaB protein. A typical iodide quenching analysis of the Trp emission spectrum for DnaB helicase showed a systematic quenching and a blue shift of the emission maxima with increasing iodide concentration (Figure 3A). Titrations were carried out at two concentration ranges: a low concentration range (0−0.25 M) and a high concentration range (0.05−0.5 M). Analysis by Stern−Volmer plot (F_0/F vs [iodide]) displayed a downward curvature with increasing concentrations of quencher at both high and low concentration ranges of iodide regardless if the total K^+ was held constant. (Figure 3B,C). A downward

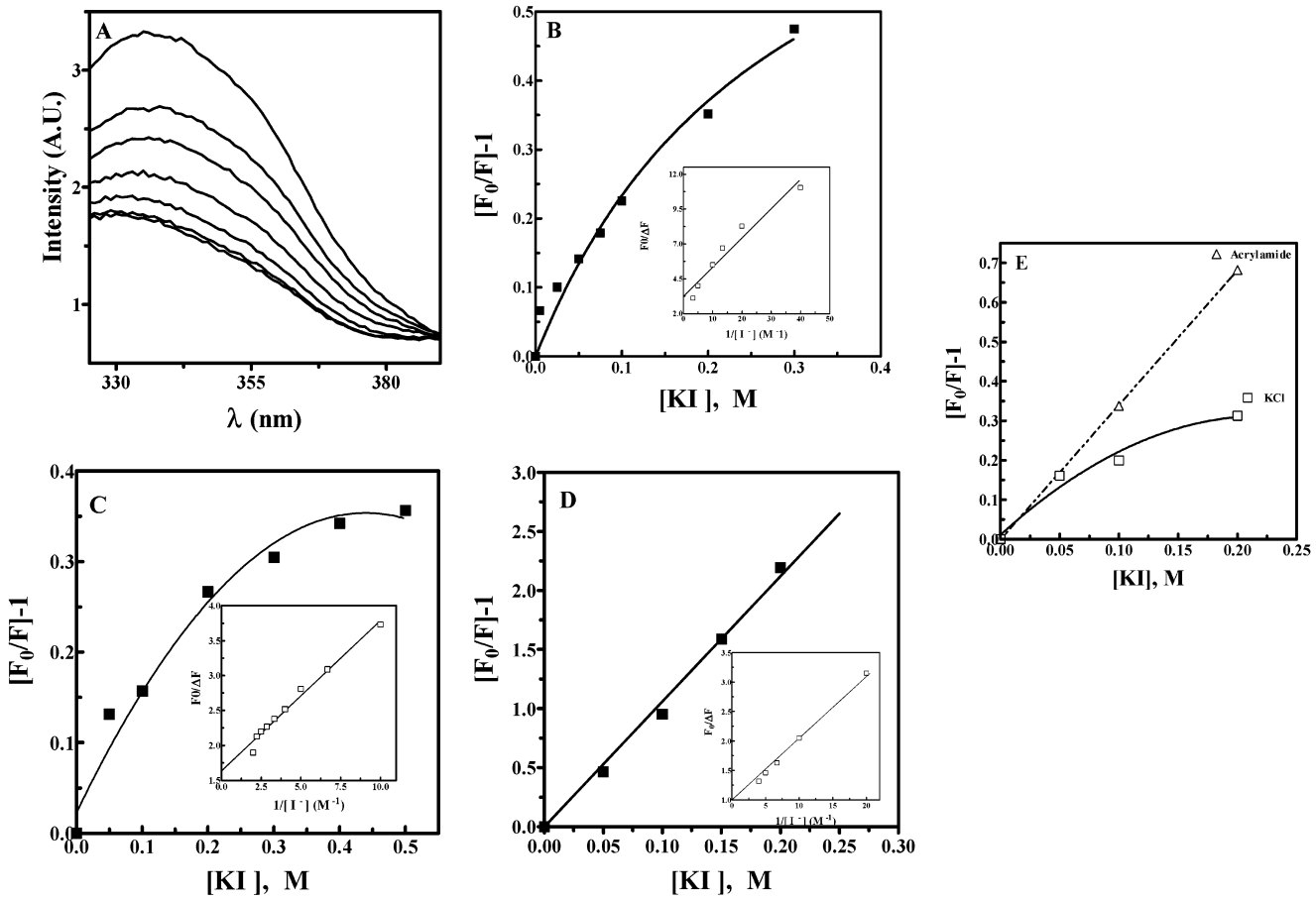

FIGURE 3: Fluorescence spectra of DnaB helicase and titration with potassium iodide. (A) Fluorescence spectra of DnaB helicase and titration with KI. The KI titrations were carried out as described in Materials and Methods. (B) Stern−Volmer plot $\{(F_0/F) - 1$ vs [KI]$\}$ for DnaB (100 μg protein/mL). Titrations were carried out in at a range of 0−0.05 M KI. The inset is the Lehrer modification $\{F_0/\Delta F$ vs 1/[KI]$\}$ of this Stern−Volmer plot [or Lehrer plot] used here to calculate the solvent accessible fractions of tryptophan residues in DnaB helicase. (C) Stern−Volmer plot of DnaB (100 μg/mL) carried out in at a range of 0−0.5 M KI. The inset is the Lehrer plot. (D) Stern−Volmer plot of denatured DnaB (100 μg protein/mL) carried out in the range of 0−0.5 M KI. The inset is the Lehrer plot. (E) Comparison of acrylamide (△) vs KI (□) quenching of DnaB. Data for each titration were analyzed by least-squares regression analysis using PRISM 3.02 from Graph pad Corporation, CA.

curvature in Stern−Volmer plot is a characteristic of tryptophan residues located in hydrophobic environments and are less accessible to water as well as iodide (*28*).

The Lehrer equation (eq 2) and the derived plot of $[F_0/\Delta F]$ versus 1/[Q] were used to quantitate the fractional solvent accessibility (f_a) and a gross estimate of the approximate number of Trp residues in hydrophobic environment. It should be noted that the contributions of each of the three Trp residues to the total fluorescence are not equal. In fact, Trp294 appeared to be the major contributor, and Trp48 and Trp456 are minor contributors to the total fluorescence that was inferred from a deduced fluorescence spectrum of individual Trp residues, which has been discussed in detail later. Titration of the DnaB helicase with iodide in the low concentration range (0−0.25 M) gave a maximum quenching of 31%. It should be noted that a complete quenching of fluorescence of a fully exposed Trp residue in this study led to an 87% diminution of the emission intensity (data not shown) and the remaining 13% cannot be quenched. Thus, a 31% quenching is equivalent to one residue quenching (Figure 3B inset). The K_a for DnaB was calculated to be 4.7 M^{-1}. Another 2-fold increase in the concentration of iodide raised the accessibility of tryptophan to 62%, thus reflecting a quenching of two Trp residues (Figure 3C inset). The K_a was decreased to 2.8 M^{-1}.

To determine if the observed changes in fluorescence described above are truly related to changes in the conformation of the DnaB protein, it was denatured in 7 M urea and titrated with iodide. In 7 M urea, the protein is totally unfolded, and Trp residues should be freely accessible to the solvent, leading to a linear quench curve (*28*). Indeed the Stern−Volmer plot for denatured DnaB was linear (Figure 3D). A further confirmation of complete solvent exposure of Trp residues in a denatured state was demonstrated by a linear Lehrer plot with an intercept of ∼1 (Figure 3D inset). The K_a was found to be 11.4 M^{-1}. This analysis of the quenching data with both native and denatured DnaB indicated the presence of one or more buried or inaccessible Trp residue (*28*, *29*).

To determine if the downward curvature displayed is a result of ionic shielding by KI, a comparison between KI and acrylamide quenching was carried out at a constant concentration ionic strength. Titration of DnaB helicase resulted in a downward curvature, suggestive of buried trpytophan residues. On the other hand, when DnaB was quenched with acrylamide a linear curve was obtained. The explanation for the differences seen between KI and acrylamide is the acrylamide being a neutral quencher is able to penetrate further in hydrophobic regions within the DnaB and quench trpytophan that are not accessible to KI.

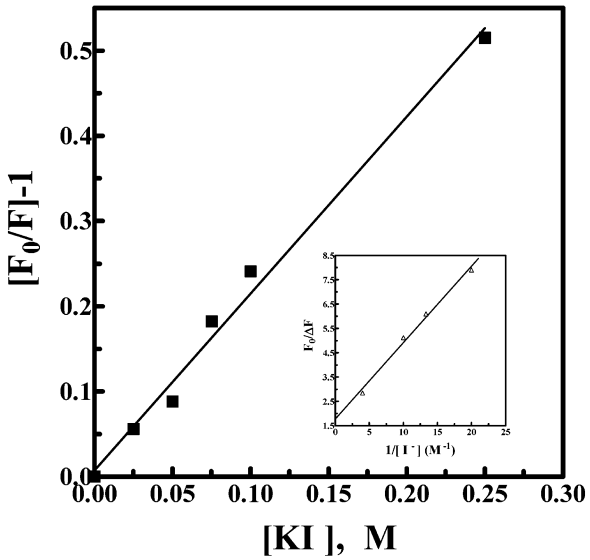

FIGURE 4: Titration of DnaB mutants. The Stern−Volmer plot of C-terminal truncated mutant DnaBΔ1. The inset is the Lehrer plot for DnaBΔ1. The KI titrations were carried out as described in Materials and Methods. Data for each titration were analyzed by least-squares regression analysis using PRISM 3.0 from Graph pad Corporation, San Diego, CA. The inset is the Lehrer plot for DnaBΔ3.

Quenching Analysis of DnaB Mutants and Assignment of Individual Trp Environments. To assess the environment of individual tryptophan residue, quenching analyses on deletion and W → C site-specific mutants of DnaB helicase were performed. We created two deletion mutants of DnaB. The DnaBΔ1deletion has been described earlier (*25*) and lacks the C-terminal tryptophan (W48). For DnaBΔ1, a linear Stern−Volmer plot was obtained suggesting greater solvent accessibility of the two remaining residues: Trp294 and Trp456 (Figure 4). The Lehrer plot was linear with a *y*-intercept of ∼1, demonstrating similar solvent accessibilities of the two remaining Trp residues (Figure 4 inset). The K_a for DnaBΔ1 was found to be 2.0 M^{-1}.

Deletion mutants can be associated with many aberrations including structural alterations and improper folding. Therefore, to further characterize the fluorescence and quenching characteristics of Trp residues, we have created three single tryptophan to cysteine mutants: W48C, W294C, and W456C. With the single W → C mutants, a difference in accessibility to quenching was seen when wild-type DnaB was compared to the cysteine mutants (Figure 5A). The linear Stern−Volmer plot of the W48C mutant suggests that there was an equal accessibility of the two remaining tryptophan residues, W294 and W456. The K_a for W48C mutant was calculated to be 2.2 M^{-1}, and accessibility was found to be 100%. With both W294C and W456C mutants, decreased rates of quenching were observed. For W294C the accessibility was found to be 76% with a K_a of 2.0 M^{-1}, while the W456C mutant was found to have an accessibility of 71% with a K_a of 1.5 M^{-1}. Therefore, both of these mutants appear indistinguishable in fluorescence quenching analysis.

The W → C mutant proteins were utilized to construct spectrum for individual Trp residues by difference spectrum analysis. Trp294 appeared to be the major contributor to the fluorescence spectrum of DnaB (Figure 5B). Trp456 was the lowest contributor to the overall fluorescence.

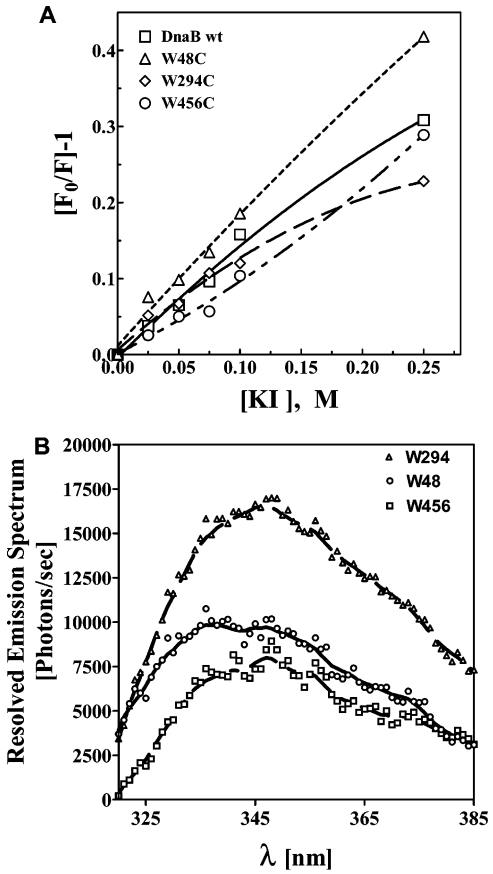

FIGURE 5: Fluorescence quenching analysis of site-directed tryptophan (W → C) mutants. (A) Stern−Volmer plot of DnaB mutants W48C, W294C, and W456C, (100 μg protein/mL) carried out in the range of 0−0.50 M KI. (inset) The Lehrer plot. The KI titrations were carried out as described in Materials and Methods. Data for each titration were analyzed by least-squares regression analysis using PRISM 3.0. (B) Computed spectrum of the relative contribution of each Trp residues to the overall spectrum of DnaB. Each spectrum was computed by subtraction of respective W → C DnaB mutant spectrum from that of wild-type DnaB spectrum: W294 (△) W48 (○) and W456 (□).

Effects of Nucleotide Binding on the Conformation of DnaB Helicase. The DnaB protein is a DNA-dependent ATPase, and the bound ATP is rapidly hydrolyzed making the DNAB·ATP complex virtually transient. In contrast, ATPγS is not hydrolyzed and forms a stable complex with the DnaB protein and is thus more suitable for equilibrium fluorescence studies. We examined changes in the tryptophan quenching of DnaB protein complexed with nucleotides in order to determine any changes in the solvent accessibility of Trp residues and quenching properties upon nucleotide binding. These results could be used to identify conformational changes in its three domains as a result of substrate binding. DnaB helicase was titrated with iodide in the presence of either 1 mM ATPγS or ADP. Titration of KI in the presence of ATPγS alone resulted in a significant change in the Stern−Volmer plot with an upward curvature (Figure 6). The upward curvature is indicative of a combined static and collisional (dynamic) quenching (*28*, *29*). Increased rates of both static and collisional quenching were also observed when DnaB was titrated in the presence ADP or ATPγS (Figure 6). Since we determined that W294 and W456 were fairly accessible to solvent, the observed static quenching with either ADP or ATPγS may not necessarily be due to direct quenching of Trp294 that is located within the

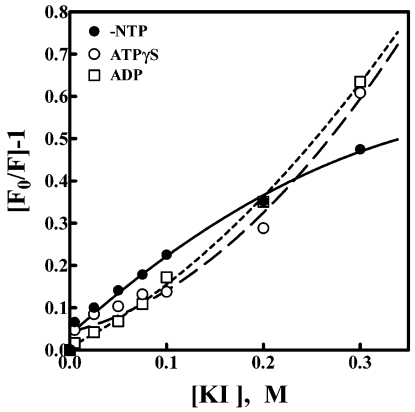

FIGURE 6: KI Titration of DnaB in the presence of nucleotide. DnaB titrations, using KI, as described in Materials and Methods. Titrations were carried out with DnaB alone (●) and in the presence of ATP γS (○) and ADP (□). Changes in the quenching efficiency were seen with all three. The KI titrations were carried out as described in Materials and Methods. Data for each titration were analyzed by nonlinear least-squares regression analysis using PRISM 3.0.

nucleotide-binding domain. It is more than likely that the most hydrophobic Trp48 in domain α may account for the dramatic change observed here due to an accompanying conformational change in the α domain of the protein. The quench curve (Figure 6) also indicated that a major conformational transition occurs upon ADP and ATPγS binding. These nucleotide-binding events led to significant changes in the orientation of the Trp residue(s) from a hydrophobic to hydrophilic environment and increased solvent exposure. A similar change in the Stern−Volmer plot from a downward curve to a straight line was reported for cAMP receptor protein upon cAMP binding by Wasylewski et al. (*31*). Consequently, a major conformational change is probable in the α domain upon nucleotide binding.

Conformational Changes of DnaB Helicase Associated with DNA Binding. To determine the effects of DNA binding on the conformations of DnaB helicase, Trp fluorescence quenching analysis was carried out with oligo(dT)$_{25}$ in the presence of ADP or ATPγS (Figure 7).

The DnaB·DNA complexes were formed at low salt concentration (~100 mM KCl or KI). The complex remained stable at high salt, as determined by ssDNA−cellulose chromatography and polarization analysis. In fact, Arai and Kornberg (*26*) have demonstrated that a ternary DnaB-DNA-ATPγS complex can be stable up to 2M NaCl. DnaB titration with iodide in the presence of oligo(dT)$_{25}$ alone indicated a combination of static and collisional/dynamic quenching (Figure 7). However, overall quenching was significantly reduced when compared to that observed in the presence of ADP or ATPγS, suggesting a transition to an altered conformation that reduces solvent exposure to the Trp residues. On the other hand, the quenching profile of DnaB in the presence of both ATPγS and oligo(dT)$_{25}$ showed a downward pattern similar to that observed with ligand-free DnaB, indicating that the conformation is similar to the native conformation of DnaB (conformation I). This quench curve is significantly different from that observed for ATPγS alone (Figure 6). Quenching analysis of a ternary complex of DnaB with ADP generated a quench curve that was similar to that observed with ADP alone but significantly different from that observed with ATPγS and oligo(dT)$_{25}$. The Stern−

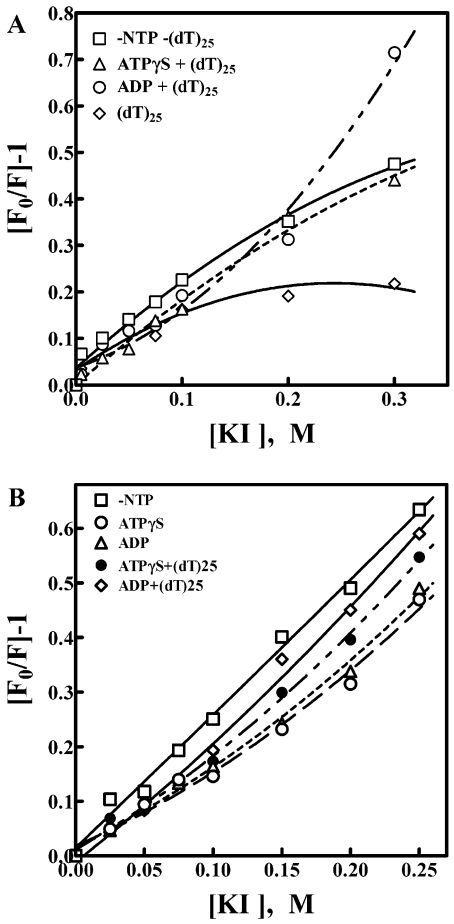

FIGURE 7: KI Titration of DnaB wild type and W48C mutant in the presence of nucleotide and DNA. (A) Titrations with KI were carried out with DnaB alone (□), ADP + oligo(dT)$_{25}$ (○), ATPγS oligo(dT)$_{25}$ (△), and oligo(dT)$_{25}$ alone (◇). (B) Titrations with KI were carried out with W48C mutant alone (□), ATPγS (○), ADP (△), ADP + oligo(dT)$_{25}$ (◇), and ATPγS oligo(dT)$_{25}$ (●). The KI titrations were carried out as described in the Materials and Methods. Data for each titration were analyzed by nonlinear least-squares regression analysis using PRISM 3.02 from Graph pad Corporation, CA.

Volmer plot with ADP alone indicated that the most open conformation with maximum accessibility of Trp residues was that of the DnaB·ADP complex. The binding to DNA or oligonucleotide in the presence of ADP did not alter the open conformational state of DnaB any further.

Results of the quenching analysis indicated that Trp48 in domain α of DnaB is in the most hydrophobic environment among the three Trp residues. Therefore, the conformational changes observed with DNA and nucleotide binding would likely involve a change in the environment of Trp 48 only. We have further analyzed conformational changes associated with the W48C mutant of DnaB when DNA and nucleotide were bound. Results of quenching analysis by the Stern−Volmer equation are shown in Figure 5A. In the absence of DNA and nucleotides, W48C mutant exhibited a linear Stern−Volmer plot. In the presence of nucleotide or DNA, Stern−Volmer plots with an upward curvature, and a small attenuation of Trp fluorescence quenching was observed in each case. Thus, the major conformational change observed with wild-type DnaB was due to Trp48 in the α domain. The minor conformational change observed with W48C mutant can be attributed to the remaining two Trp residues, Trp294 and Trp456.

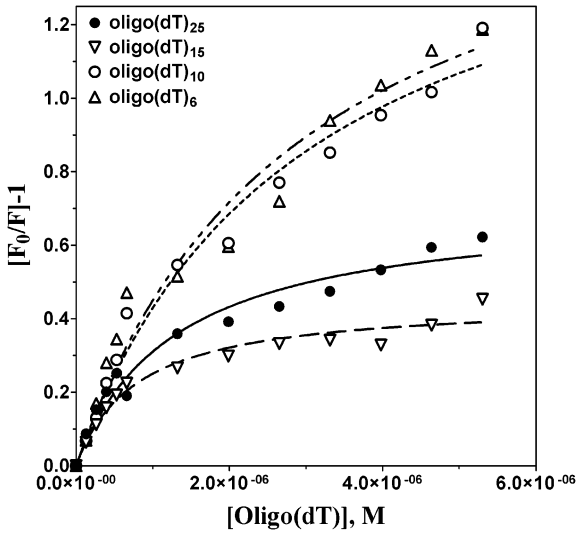

FIGURE 8: DNA Titration of DnaB in the presence of 100 mM KI. (A) DnaB helicase was titrated, in the presence of 100 mM KI, with various oligonucleotides oligo(dT)$_6$ (△), oligo(dT)$_{10}$ (○), oligo(dT)$_{15}$ (▽), and oligo(dT)$_{25}$ (●). Difference of both the accessibility of tryptophan and the rate of quenching was seen between larger and smaller sized oligonucleotides. Data for each titration were analyzed by least-squares regression analysis using PRISM 3.02 from Graph pad Corporation, CA.

Influence of Oligonucleotide Length on the DNA Binding Affinity. Binding to oligonucleotides appeared to have significant influence on the conformation of DnaB hexamer, as determined from Trp fluorescence quenching. Therefore, we decided to study the effects of oligonucleotide length on Trp fluorescence quenching. As discussed earlier, one of the three Trp groups is exposed and can be quenched at a very low KI concentration and a second Trp group is partially exposed and is partially quenched at a low KI concentration (≤100 mM). Therefore, the concentration of KI was kept constant at 100 mM so that exposed tryptophan residues could become accessible to iodide quenching. Titrations and fluorescence quenching analyses were performed using oligo(dT) of various sizes: (dT)$_6$, (dT)$_{10}$, (dT)$_{15}$, and (dT)$_{25}$ (Figure 8). In general, with all four oligonucleotides, binding to DnaB helicase caused significant quenching of Trp fluorescence. Quenching curves observed with both oligo(dT)$_{25}$ and oligo(dT)$_{15}$ were found to be quite comparable. However, the shorter oligonucleotides (dT)$_{10}$ and (dT)$_6$ were found to quench Trp fluorescence to a greater extent than both oligo(dT)$_{25}$ and oligo(dT)$_{15}$. The Lehrer equation (eq 2) was used to calculate tryptophan accessibility. The calculated Trp accessibility values were as follows: 38% for oligo(dT)$_{25}$, 31% oligo(dT)$_{15}$, 55% for oligo(dT)$_6$, and 60% for oligo(dT)$_{10}$.

Homology-Based Modeling of DnaB Helicase. The amino acid sequence of domains β and γ of DnaB helicase were aligned with the helicase domain of the gene 4 helicase-primase of bacteriophage T7, and the alignment is shown in Figure 9. The alignment indicated that there is significant homology between these two polypeptides, so that the atomic coordinates from the protein data bank for these proteins can be used for homology-based modeling. This alignment indicated that the identity within the aligned domain is ~30% and the similarity was ~40%.

The X-ray crystal structure of the domain α has been solved by Fass et al. (*32*). A ribbon diagram of this domain is shown in Figure 10. The Trp48 residue is located in the α domain. We have explored the molecular environment of this tryptophan using the X-ray structure, and the hydrophobic groups around Trp48 are highlighted in red in Figure 10. These groups appear to form a hydrophobic pocket that makes theTrp48 solvent inaccessible and resistant to quenching.

The X-ray structure of the remainder of the DnaB polypeptide is not available. Therefore, we have generated a model for the $\beta\gamma$ domains of DnaB (Figure 11) using its homology with T7 gene4B helicase and homology-based protein structure modeling softwares (Swiss PDB and SYBYL6.7). The X-ray structure of the helicase domain of T7 gene 4 helicase-primase has been solved by Sawaya et al. (*40*), and the atomic coordinates are available from the Protein Data Bank (PDB code 1CR0). The Trp294 residue is in domain β (highlighted in red) as shown in Figure 9C. The Trp294 appears to be in a partially hydrophobic environment and correlates well with the results of quenching analysis of solvent accessibility and quenching efficiency of Trp294. We could not model the C-terminal end of the protein; as a result, the modeled region did not include Trp456. However, Trp456 is at the very end of the C-terminal and the environment of this Trp residue would likely be hydrophilic.

DISCUSSION

Structural Domains of DnaB Helicase. DnaB helicase is the primary replicative DNA helicase in *E. coli* (*1*). It is also prototype of all replicative DNA helicases in prokaryotes and eukaryotes. Although, we have gained a basic under-

```
DnaB 196   LFQ..QPHDG VTGVNTGYDD LNKKTAGLQP SDLIIVAARP SMGKTTFAMN
T7   280   IREHLSSEES VGLLFSGCTG INDKTLGARG GEVIMVTSGS GMGKSTFVRQ

DnaB 244   LVENAAMLQD KPVLIFSLEM PSEQIMMRSL ASLSRVDQTK IRTGQLDDED
T7   329   QALQWGTAMG KKVGLAMLEE SVEETAEDLI GLHNRVRLRQ SDSLKREIIE

DnaB 294   WARISGTMGI LLEKRNIYID DSSGLTPTEV RSRARRIARE HGGIG..LIM
T7   379   NGKFDQWFDE LFGNDTFHLY DSFAEAETD. RLLA.KLAYM RSGLGCDVII

DnaB 342   IDYLQL.MRV PALSDNRTLE IAEISRSLKA LAKELNVPVV ALSQLNRSLE
T7   427   LDHISIVVSA SGESDERKM. IDNLMTKLKG FAKSTGVVLV VICHLKNPDK

DnaB 390   QRA..DKRPV N.SDLRESGS IEQDADLIMF IYR
T7   476   GKAHEEGRPV SITDLRGSGA LRQLSDTIIA LER
```

FIGURE 9: Homology of DnaB helicase and T7 gene 4B DNA helicase. Homology of the domain $\beta\gamma$ of DnaB helicase with gene 4B DNA helicase of bacteriophage T7, the X-ray structure of which has been solved (PDB code 1CR0).

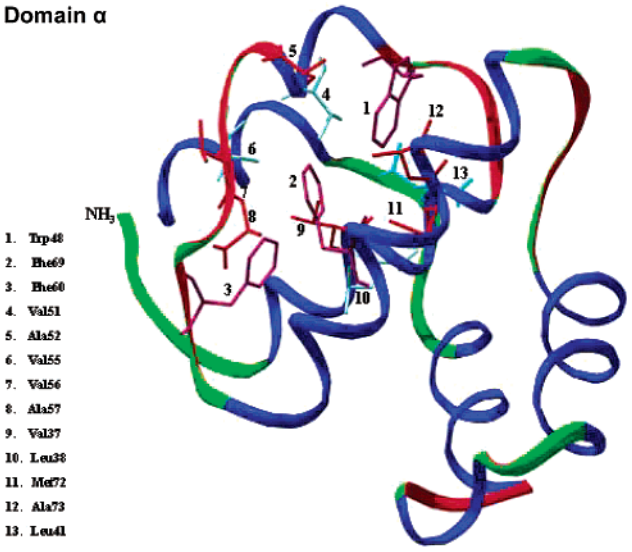

FIGURE 10: Structure of the α domain. X-ray structure of the α domain with atomic coordinates reported by Fass et al. (*32*). The residues that form the "hydrophobic core" involving the indole side chain of W48 are highlighted in red. The Trp48, Phe60, and phe69, all highlighted in magenta color, appears to stack to each other, which may reduce fluorescence quantum yield of Trp48.

standing of its hexameric structure and enzymatic functions during last two decades, very little is known regarding DNA unwinding (*1*−*10*). The mechanism by which the energy of nucleotide hydrolysis is transduced into DNA melting remains unknown. We defined earlier three functional domains of DnaB helicase: domain α, amino acid residues (aa) 1−156; domain β, aa 157−302; and domain γ, aa 302−471 (*24*, *25*). Among these three domains of DnaB helicase, domain α is the least conserved (∼19%) domain, and domain γ is the most conserved (∼60%). Similar domain structures have been proposed for a number of other multimeric proteins that form high-order nucleoprotein complexes such as bacteriophage Mu transposase and retroviral integrase, RNA helicases, etc. (*35*−*37*). Understanding the functions of individual domains greatly aided in the structure−function analysis of these enzymes.

Structural studies of DnaB demonstrated that domain β is the nucleotide binding and hydrolysis domain; the domain γ is both a dimerization and DNA binding domain. The domain α is essential for DNA helicase function but not for hexamer formation, ATPase activity, and DNA binding (*34*). It is also least conserved with no detectable functional motif. Consequently, we proposed a mechanical function of this domain that aids the hexamer in unwinding duplex DNA (*24*, *25*). However, it is expected that the conformational changes during DNA unwinding may be only local changes in a single domain and not large enough for detection by methods such as circular dichroism spectroscopy. Therefore, to detect smaller conformational changes, an internal probe for analyzing structural and conformational changes during various steps in DNA helicase and ATPase activities appeared necessary. Each of the three functional domains (α, β, and γ) of DnaB helicase harbors a unique Trp residue (*9*, *10*). Consequently, intrinsic tryptophan fluorescence is an ideal tool in this case to examine any structural or conformational changes during various enzymatic steps of DnaB helicase.

Analysis of Molecular Environments of Tryptophan Residues of DnaB Helicase. We have utilized these uniquely located Trp residues and very sensitive intrinsic Trp fluorescence to delineate conformational transition(s) in the DnaB protein associated with various steps in the mechanism of its helicase action. The environments and fluorescence characteristics of each of these Trp residues were examined by fluorescence quenching analysis coupled with site-directed and deletional mutagenesis. Analysis of fluorescence quench-

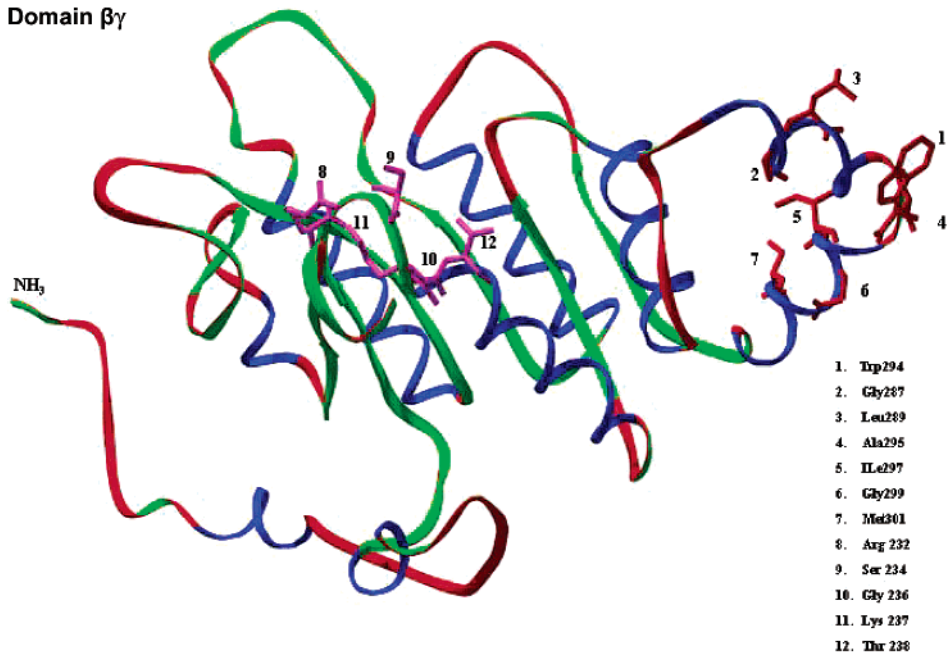

FIGURE 11: Structure of the $\beta\gamma$ domains by homology modeling. Homology modeling of domains $\beta\gamma$ using SYBYL 6.7 (Tripos Inc., St Louis, MO.) using the atomic coordinates from the X-ray structure of the helicase domain of gene 4 DNA helicase/primase of bacteriophage T7 as described by Sawaya et al. (*40*). The residues that contribute to a partial hydrophobic environment near Trp256 are highlighted in red. The residues in the Walker A motif, Ala231, Ser234, Gly236, Lys237, and Thr238 are highlighted in pink color. This is the putative ATP binding pocket of the DnaB helicase.

Scheme 1: Four Putative Conformational States Involved in Substrate Binding and Helicase Action

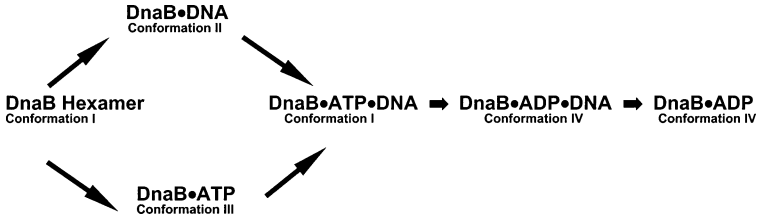

ing data of DnaB protein by the Stern−Volmer equation generated a nonlinear plot with a downward curvature (Figure 3). Downward curvatures in the Stern−Volmer plot are a general and qualitative indication of buried or solvent inaccessible tryptophan residues in proteins and have been described in detail by Lakowicz (*28*). The Lehrer equation and plot allow quantitative determination of solvent inaccessibility, providing diagnostic information of the Trp environments. The linear curve seen with acrylamide is consistent with prior studies (*38*). The explanation of the differences seen between KI and acrylamide is the acrylamide being a neutral quencher able to penetrate further in hydrophobic regions within the DnaB and quench trpytophan that are not accessible to KI.

On the basis of the tryptophan quenching data from wild type and mutant DnaB proteins, it is probable that at least one residue is located on or near the surface of the helicase. This tryptophan is readily accessible to even low concentrations of iodide. The second tryptophan is slightly accessible upon titration with higher concentrations of iodide. A third residue is buried and is accessible to iodide only when the protein is denatured with 7M urea. The DnaBΔ1 mutant, which lacks Trp48 in the α domain, revealed that the C-terminal Trp residues (Trp294, and Trp456) are more readily accessible to solvent and also iodide.

Since we observed increased solvent accessibility with DnaBW48C mutant as compared to W294C and W456C, it is reasonable to conclude that the two remaining tryptophan residues found in W48C are more accessible to solvent and quencher, making the Trp48 the least solvent accessible tryptophan. Therefore, our studies indicate that one Trp residue (Trp48) is nearly inaccessible and was not quenched by iodide; the second Trp residue (Trp294) is moderately inaccessible and was quenched at higher iodide concentrations, while the third Trp residue (Trp456) was likely the most accessible. The results from quenching studies with DnaB deletion mutants and W → C site-specific mutants appeared to correlate well with this assignment of the local molecular environments of these Trp residues. In addition, our determination that Trp48 is totally buried, and solvent inaccessible correlates well with the structure of N-terminal α domain determined by X-ray crystallography, which clearly pointed to the fact that Trp48 is indeed deeply buried within a hydrophobic pocket (*32*).

Conformational Transitions Associated with Oligonucleotide and Nucleotide Binding. Fluorescence quenching titration of DnaB with iodide, in the presence and absence of nucleotides and/or DNA, was designed to obtain information regarding conformational transitions associated with the binding of ATP and DNA. As described earlier, we obtained a nonlinear Stern−Volmer plot with a downward curvature with DnaB alone, indicating buried and solvent inaccessible Trp residues. Upon ADP or ATPγS binding, the Stern−Volmer plot changed dramatically from a downward to upward curvature of DnaB alone (Figure 6). The major change in the quenching curve observed here most likely indicates opening of the α domain and the subsequent exposure of the Trp48 residue to solvent as well as iodide leading to quenching. Thus, DnaB and nucleotide-bound DnaB have different conformational states. Quenching analysis of DnaB in the presence of oligonucleotides or ATPγS showed an upward curvature, indicating a combination of static and collisional or dynamic quenching (*28*). It should be noted that there is no significant quenching of tryptophan fluorescence with DNA binding in the absence of KI due to reasons such as fluorescence resonance energy transfer (data not shown). Therefore, the observed changes are due to KI quenching. When a similar analysis was performed in the presence of both ATPγS and oligonucleotides leading to a ternary complex, the curvature of the quenching changed to downward unlike that observed with ATPγS alone. In fact, the curve was closely comparable to DnaB itself (Figure 7). Therefore, the DnaB·ATPγS·DNA ternary complex has a conformational state similar to that of DnaB alone. We believe that the conformational state would remain same when ATP replaces ATPγS. Quenching analysis of DnaB in the presence of both DNA and ADP indicated that the quenching curve of this complex was similar to that observed with DnaB and ADP. Therefore, the structure of either DnaB·ADP or the DnaB·ADP·DNA complex is an open or more relaxed form. Alternatively, ADP may have inhibited DNA binding, and as a result, the conformational state of the DnaB·ADP complex remained unaltered. It should be noted that the conformational changes of DnaB detected by fluorescence quenching analysis are not necessarily large. Moreover, the changes are likely local and small but important for functions of the enzyme. In the presence of 100 mM KI, we observed changes in the Stern−Volmer plots of DnaB to depend somewhat on the lengths of the bound oligonucleotides. The higher efficiency of quenching and tryptophan accessibility were seen with smaller lengths of oligonucleotides such as 6 and 10, which can be attributed to their ability to occupy more DNA binding sites within the hexamer unlike the longer oligonucleotides. A possible explanation would be that with more DNA binding sites occupied, the protein undergoes a greater degree of conformational change resulting in increased efficiency of fluorescence quenching.

Four Identifiable Conformational States of DnaB Helicase. We found a minimum of four distinguishable conformational states of DnaB: (i) DnaB alone with a nonlinear Stern−Volmer plot with downward curvature (normal conformation I); (ii) DnaB·DNA with nonlinear Stern−Volmer plot with upward curvature (conformation II); (iii) DnaB·ATPγS with nonlinear Stern−Volmer plot with upward curvature and increased quenching efficiency (conformation III); and (iv)

DnaB·ADP with nonlinear Stern−Volmer plot with upward curvature and maximum quenching (conformation IV). We believe that DnaB·ATP would also have conformation III because of concave Stern−Volmer plot. In the presence of DNA and ATPγS, DnaB would be in a conformation similar to the normal conformation. However, in the presence of ADP and DNA, DnaB would be in conformation IV. Therefore, when the DnaB·ATP·DNA complex is converted to the DnaB·ADP·DNA complex due to ATP hydrolysis, the conformation of DnaB changes from conformation I to conformation IV. The dissociation of the DnaB·ADP·DNA complex would release DnaB protein from the complex state to free form and this change likely results in a change from conformation IV to conformation I. Conformation I is likely the most conducive conformation for DNA and ATP binding. Consequently, our results suggest that these four basic conformational states are important in governing the functions of DnaB helicase. Our results also indicate that DNA and ATP binding to DnaB are independent events, with each step contributing its own conformational changes. Moreover, DnaB undergoes conformational transitions differentially with respect to these substrates. Incidentally, the sedimentation coefficient of DnaB hexamer changes upon nucleotide and DNA binding that also indicated probable structural or conformational changes (*42*). In addition, electron microscopic analysis by Egelman et al. indicated that DnaB has different quaternary structures upon nucleotide and DNA binding (*43*). Earlier studies by Arai and Kornberg (*2*) have also shown a maximum of 3.6 oligonucleotides per hexamer. However, Jezeweska et al. (*42*) found one oligonucleotide binding per hexamer using fluorescence studies. This discrepancy between various DNA binding studies remains unresolved.

Roles of the Conformational States in the DNA Unwinding. A coherent model of DNA unwinding and the energy transduction of nucleotide hydrolysis have not been established (*3*). However, a number of models have been proposed and reviewed by Patel and Picha (*3*). Earlier, we have proposed a three-site model based on our studies (*25*). There is one common theme in all of these models that requires conformational change due to ATP binding that allows binding to DNA and another conformational change due to conversion of ATP to ADP that promotes DNA release. We have proposed a model of this single cycle of DNA binding and ATP hydrolysis in a cartoon as shown in Scheme 1 and correlated the independent interactions seen with ATP, ADP, and DNA with four possible conformational states, depending on the substrates and cofactors. DnaB exists in a normal form (conformation I) until DNA or ATP is bound. Upon DNA binding in the absence of nucleotides (ATPγS or ADP), the helicase undergoes a conformational change to conformation II (taut conformation), in which Trp residues are less accessible to solvent and fluorescence quenching. Upon ATP binding, DnaB undergoes a different type of conformational change to conformation III (open conformation I), in which Trp residues are more accessible to solvent and fluorescence quenching. Finally, the formation of DnaB·ATP·DNA ternary complex returns DnaB to its native conformation or conformation I. Once ATP is hydrolyzed leading to the formation of DnaB·ADP·DNA ternary complex, DnaB undergoes a conformational change to conformation IV (Open conformation II), in which Trp residues are most accessible to the solvent and fluorescence quenching. Release of the bound DNA results in the formation of the DnaB·ADP binary complex, whose conformation is similar to that of DnaB·ADP·DNA ternary complex or conformation IV. Release of ADP returns DnaB to the native conformation I, allowing for the cycle to be repeated. The quenching studies carried out with DnaBW48C mutants in the presence of various ligands (Figure 7B) indicated that the Stern−Volmer plots remain relatively unchanged. Therefore, the conformational dynamics with ligand binding events appear to be due to Trp48 and the domain α. In conclusion, the results presented here show that DnaB helicase has at least four identifiable conformational states that depend on the state of ligand or substrate binding and indicate their unique role in the transduction of the energy of ATP hydrolysis to duplex DNA unwinding.

Structural Models of DnaB Helicase. Crystal structures of enzymes greatly facilitate detailed understanding of the mechanism of action of complex enzymes (*40*, *41*). Determination of structure of RNA polymerase II, another complex enzyme, established its unique DNA binding mechanism (*41*). Unfortunately, the crystal structure of complete DnaB helicase has not been solved in the last 20 years, primarily due to the fact that the DnaB protein crystals do not diffract (Biswas, S., and Amzel, A. M., unpublished observation). However, the structure of the α domain has been resolved (*32*). In addition, the crystal structure of T7 bacteriophage DNA helicase has also been reported recently (*40*). Therefore, we have utilized available X-ray coordinates of these polypeptides and homology-based molecular modeling techniques to decipher the partial structures of the DnaB helicase. The partial structural models of the three domains of DnaB are presented in Figures 10 and 11 in order to correlate the results of tryptophan fluorescence quenching analysis with the three-dimensional structure and deduced environments of each of these Trp residues. The X-ray structure of α domain and the modeled structure of the $\beta\gamma$ domain allow comparison of at least two of the three Trp residues. For Trp48 and Trp294, the structural environments of these residues, computed from these structural models, appear to agree well with the deduced environments of these residues from the fluorescence quenching analysis.

In the hexameric state of DnaB helicase, it is possible that the hydrophobic pockets in the six α domains involving Trp48 residues (Figure 10) interact, especially upon DNA binding, and form a hydrophobic ring that encircle the DNA. Perhaps the hexameric substructure involving the α domains opens and closes in response to binding of substrates and ATP hydrolysis in order to transduce the energy of ATP hydrolysis to mechanical movement of DNA strand. In summary, this model represents a possible role of the α domain in the energy transduction process.

ACKNOWLEDGMENT

We thank Dr. Robert Nagele of this University for the critical review of this manuscript.

REFERENCES

1. Kornberg, A., and Baker, T. A (1992) *DNA Replication*, W. H. Freeman and Co., New York.
2. Arai, K., and Kornberg, A. (1981) *J. Biol. Chem. 256*, 5253−5259.

3. Patel, S. S., and Picha, K. M. (2000) *Annu. Rev. Biochem. 69*, 651−697.
4. Nakayama, N., Arai, N., Kaziro, Y., and Arai, K. A. (1984) *J. Biol. Chem. 259*, 88−96.
5. LeBowitz, J. H., and McMacken, R. (1986) *J. Biol. Chem. 261*, 4738−4748.
6. Alfano, C., and McMacken, R. (1989) *J. Biol. Chem. 264*, 10699−106708.
7. Biswas, S. B., and Biswas, E. E. (1987) *J. Biol. Chem. 262*, 7831−7838.
8. Biswas, E. E., Chen, P.-H., and Biswas, S. B. (1994) *Biochemistry 33*, 11307−11314.
9. Wickner, S., and Hurwitz, J. (1975) *Proc. Natl. Acad. Sci. U.S.A. 72*, 921−925.
10. Sekimizu, K., Bramhill, D., and Kornberg, A. (1988) *J. Biol. Chem. 263*, 7124−7130.
11. Mukhopadhyay, G., Carr, K. M., Kaguni, J. M., and Chattoraj, D. K. (1993) *EMBO J. 12*, 4547−4554.
12. Odegrip, R., Schoen, S., Haggard-Lundquist, E., Park, K., and Chattoraj, D. K. (2000) *J. Virol. 74*, 4057−4063.
13. Ludlam, A. V., McNatt, M. W., Carr, K. M., and Kaguni, J. M. (2001) *J. Biol. Chem. 276*, 27345−27353.
14. Tougu, K., Peng, H., and Marians, K. J. (1994) *J. Biol. Chem. 269*, 4675−4682.
15. Mallory, J. B., Alfano, C., and McMacken, R. (1990) *J. Biol. Chem. 265*, 13297−13307.
16. Manna, A. C., Pai, K. S., Bussiere, D. E., Davies, C., White, S. W., and Bastia, D. (1996) *Cell 87*, 881−891.
17. Mensa-Wilmot, K., Seaby, R., Alfano, C., Wold, M. C., Gomes, B, and McMacken, R. (1989) *J. Biol. Chem. 264*, 2853−2861.
18. Sutton, M. D., Carr, K. M., Vicente, M., and Kaguni, J. M. (1998) *J. Biol. Chem. 273*, 34255−34262.
19. Messer, W., Blaesing, F., Jakimowicz, D., Krause, M., Majka, J., Nardmann, J., Schaper, S., Seitz, H., Speck, C., Weigel, C., Wegrzyn G., Welzeck, M., and Zakrzewska-Czerwinska, J. (2001) *Biochimie 83*, 5−12.
20. Dallmann, H. G., Kim, S., Pritchard, A. E., Marians, K. J., and McHenry, C. S. (2000) *J. Biol. Chem. 275*, 15512−15519.
21. Bhattacharyya, S., and Griep, M. A. (2000) *Biochemistry 39*, 745−752.
22. Gao, D., and McHenry, C. S. (2001) *J. Biol. Chem. 276*, 4441−4446.
23. Biswas, E. E., Biswas, S. B., and Bishop, J. M. (1986) *Biochemistry 25*, 7368−7374.
24. Biswas, E. E., and Biswas, S. B. (1999) *Biochemistry 38*, 10919−10928.
25. Biswas, E. E., and Biswas, S. B. (1999) *Biochemistry 38*, 10929−10939.
26. Arai, K., and Kornberg, A. (1981) *J. Biol. Chem. 256*, 5260−5266.
27. Sonveaux, N., Vigano, C., Shapiro, A. B., Ling, V., and Ruysschaert, J. M. (1999) *J. Biol. Chem. 274*, 17649−17654.
28. Lakowicz, J. R. (1999) *Principles of fluorescence spectroscopy*, 2nd ed., Plenum Publishers, New York, 10013.
29. Lehrer, S. S. (1971) *Biochemistry 10*, 3254−3263.
30. Biswas, E. E., Chen, P.-H., and Biswas, S. B. (1995) *Protein Expr. Purif. 6*, 763−770.
31. Wasylewski, M., Malecki, J., and Wasylewski, Z. (1995) *J. Protein Chem. 14*, 299−308.
32. Fass, D., Bogden, C. E., and Berger, J. M. (1999) *Structure 7*, 691−698.
33. Bird, L. E., Pan, H., Soultanas, P., and Wigley, D. B. (2000) *Biochemistry 39*, 171−182.
34. Biswas, S. B., Chen, P. H., and Biswas, E. E. (2002) *Nucleic Acids Res. 30*, 2809−2816.
35. Namgoong, S.-Y., Kim, K., Saxena, P., Yang, J.-Y., Jayaram, M., Giedroc, D. P., and Harshey, R. M. (1998) *J. Mol. Biol. 275*, 221−232.
36. Nakayama, C., Teplow, D. B., and Harshey, R. M. (1987) *Proc. Natl. Acad. Sci. U.S.A. 84*, 1809−1813.
37. Kim, K., and Harshey, R. M. (1995) *Nucleic Acids Res. 23*, 3937−3943.
38. Bujalowski, W., and Klonowska, M. M. (1994) *J. Biol. Chem. 269*, 31359−31371.
39. Zelent, B., Kuśba, J., Gryczynski, I., Johnson, M. L., and Lakowicz, J. R. (1998) *Biophys. Chem. 73*, 53−75.
40. Sawaya, M. R., Guo, S., Tabor, S., Richardson, C. C., and Ellenberger, T. (1999) *Cell 99*, 167−177.
41. Conaway, J. W., and Conaway, R. C. (2000) *Science 288*, 632−633.
42. Jezewska, M. J., and Bujalowski, W. (1996) *J. Biol. Chem. 271*, 4261−4265.
43. Yu, X., Jezewska, M. J., Bujalowski, W., and Egelman, E. H. (1996) *J. Mol. Biol. 259*, 7−14.

BI025992V